Living Around Active Stars
Proceedings IAU Symposium No. 328, 2016
D. Nandy, A. Valio & P. Petit, eds.

doi:10.1017/S1743921317004264

Hunting for hot Jupiters around young stars

Louise Yu[1,2] and the MaTYSSE collaboration

[1]Université de Toulouse, UPS-OMP, IRAP,
14 avenue E. Belin, Toulouse, F–31400 France
[2]CNRS, IRAP / UMR 5277,
Toulouse, 14 avenue E. Belin, F–31400 France
email: louise.yu@irap.omp.eu

Abstract. This conference paper reports the recent discoveries of two hot Jupiters (hJs) around weak-line T Tauri stars (wTTS) V830 Tau and TAP 26, through the analysis of spectropolarimetric data gathered within the Magnetic Topologies of Young Stars and the Survival of massive close-in Exoplanets (MaTYSSE) observation programme. HJs are thought to form in the outskirts of protoplanetary discs, then migrate inwards close to their host stars as a result of either planet-disc type II migration or planet-planet scattering. Looking for hJs around young forming stars provides key information on the nature and time scale of such migration processes, as well as how their migration impacts the subsequent architecture of their planetary system. Young stars are however extremely active, to the point that their radial velocity (RV) jitter is around an order of magnitude larger than the potential signatures of close-in gas giants, making them difficult to detect with velocimetry. Three techniques to filter out this activity jitter are presented here, two using Zeeman Doppler Imaging (ZDI) and one using Gaussian Process Regression (GPR).

Keywords. methods: statistical, stars: activity, stars: evolution, stars: imaging, stars: individual (V830 Tau, TAP 26), stars: magnetic fields, (stars:) planetary systems: formation, stars: pre–main-sequence, stars: rotation, stars: spots

1. Introduction

Studying young forming stars stands as our best chance to progress in our understanding of the formation and early evolution of planetary systems. For instance, detecting hot Jupiters (hJs) around young stars (1-10 Myrs) and determining their orbital properties can enable us to clarify how they form and migrate, and to better characterize the physical processes (e.g. planet-disc interaction, planet-planet scattering, Baruteau *et al.* 2014, in-situ formation, Batygin *et al.* 2016) responsible for generating such planets.

However, young stars are enormously active, rendering planet signatures in their spectra and / or light-curves extremely difficult to detect in practice. Until very recently, most planets found so far around stars younger than 20 Myr were distant planets detected with imaging techniques (e.g. β Pic b, Lagrange *et al.* 2010, and LkCa 15, Sallum *et al.* 2015). Early claims of hJs orbiting around T Tauri stars (TTSs)(e.g. TW Hya, Setiawan *et al.* 2008) finally proved to be activity signatures mistakenly interpreted as radial velocity (RV) signals from close-in giant planets (Huélamo *et al.* 2008).

Systematic exploration of hJs around TTSs, and in particular the so called weak-line T Tauri stars (wTTSs), whose accretion disc has just dissipated, is one of the main goals of the MaTYSSE (Magnetic Topologies of Young Stars and the Survival of close-in massive Exoplanets) large programme allocated on the 3.6m Canada-France-Hawaii Telescope (CFHT). This paper focuses on the study of wTTSs V830 Tau (Donati *et al.* 2016, Donati *et al.* 2017) and TAP 26 (Yu *et al.* 2017).

	V830 Tau[1]	**TAP 26**[2]
Age [Myr]	$\simeq$2.2	$\simeq$17
$M_\star$ [$M_\odot$]	1.00±0.05	1.04±0.10
$P_{\rm rot}$ [d]	2.741	0.7135
$R_\star$ [$R_\odot$]	2.0±0.2	1.17±0.17
$v \sin i$ [km.s^{-1}]	30.5±0.5	68.2±0.5
i [°]	55±10	55±10
$P_{\rm orb}$ [d]	4.927±0.008	10.79±0.14
$M \sin i$ [$M_{\rm Jup}$]	0.57±0.10	1.66±0.31
a [au]	0.057±0.001	0.0968±0.0032
a [$R_\star$]	6.1±0.6	17.8±1.3

Table 1. Summary of the properties on both hot Jupiters found within the MaTYSSE programme. From top to bottom: age, stellar mass in terms of solar masses, stellar rotation period expressed, stellar radius in terms of solar radii, line-of-sight-projected equatorial rotation velocity, inclination of stellar rotation axis to the line of sight, orbital period, minimal mass in terms of jovian masses, semimajor axis and semimajor axis in terms of stellar radii.

References:
[1] Donati *et al.* (2017)
[2] Yu *et al.* (2017)

2. Modelling the stellar activity

Targets. V830 Tau and TAP 26 are wTTSs in the Taurus stellar formation region. Their characteristics are shown in table 1.

Observations. Unpolarized (Stokes I parameter) and circularly polarized (Stokes V parameter) spectra were collected between 2015 November and 2016 February for both stars, from spectropolarimeters ESPaDOnS (Echelle SpectroPolarimetric Device for the Observation of Stars) at CFHT and Narval at TBL (Télescope Bernard Lyot). Complete information about the observations is found in Donati *et al.* (2016) and Donati *et al.* (2017) for V830 Tau and in Yu *et al.* (2017) for TAP 26.

LSD (Least Squares Deconvolution). The high value of $v \sin i$ creates a strong correlation between brightness features at the surface of the stars and distorsions within the line profiles of the unpolarized spectra. As a star rotates, these distorsions move across line profiles creating a modulation within the subsequent computed RV, following a temporal period equal to the stellar rotation period. In the presence of a hJ, the planet-induced reflex motion causes the spectrum to be blue-shifted or red-shifted as a whole, following a temporal period equal to the hJ's orbital period. LSD, a multiline technique, is applied to each spectrum in order to concentrate the information repeated in more than 7000 spectral lines into a unique profile, describing power as a function of local RV, with an SNR (signal to noise ratio) around one order of magnitude bigger than in the spectrum (see Donati *et al.* 1997b)(see Fig. 1). The global RV for each spectrum is computed as the first-order moment of the continuum-subtracted Stokes I LSD profile. Lunar pollution was corrected from some profiles.

Brightness tomography. In order to model the activity jitter of TAP 26, we applied ZDI (Semel 1989, Donati *et al.* 2014) to our data. ZDI is a tomography technique that enables to infer the bidimensional brightness distribution at the surface of the star from a time series of monodimensional LSD profiles, given the values of the rotation axis inclination to the line-of-sight, of the line-of-sight-projected equatorial rotation velocity and of differential rotation parameters. Minimizing the χ^2 and the spot coverage leads to the values of these stellar parameters (see Table 1) as well as the brightness maps which fit our data best. In the case of TAP 26, the data set was subdivided into two subsets which were fitted separately, because ZDI cannot fit the whole data set down to noise level with only one model. Figure 1 shows the time-series of TAP 26 Stokes I LSD profiles

https://doi.org/10.1017/S1743921317004264 Published online by Cambridge University Press

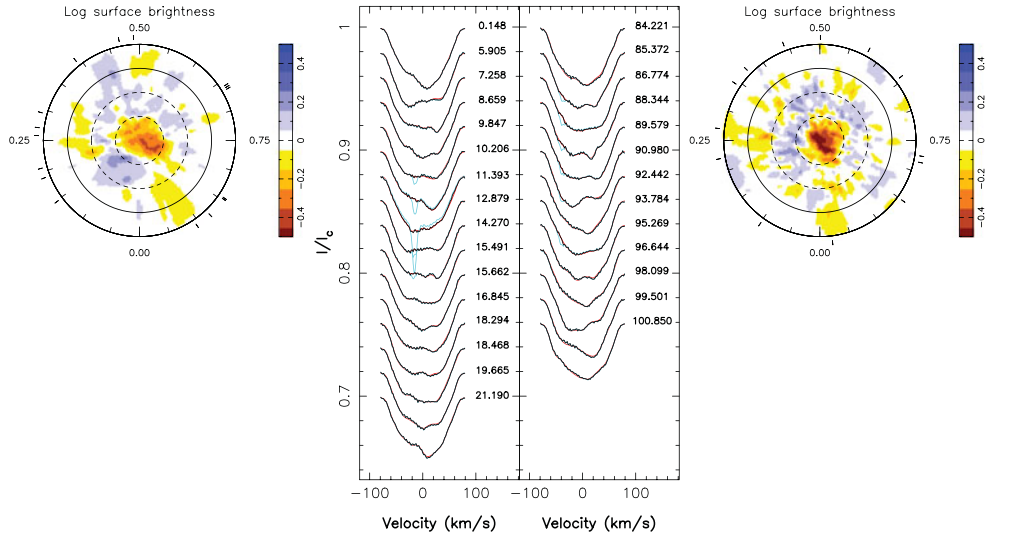

Figure 1. ZDI applied on TAP 26 data. *Center*: maximum entropy fit (thin red lines) to the observed (thick black lines) Stokes *I* LSD profiles. The 2015 Nov dataset is represented in the 1st column and the 2016 Jan dataset in the 2nd column. The Stokes *I* LSD profiles before the removal of lunar pollution are coloured in cyan. The rotational cycles are written beside their corresponding profiles, in concordance with Table 1. *Sides*: flattened polar view of the surface brightness maps for the 2015 Nov dataset (left panel) and 2016 Jan dataset (right panel). The equator and the 60°, 30° and -30° latitude parallels are depicted as solid and dashed black lines respectively. The colour scale indicates the logarithm of the relative brightness, with brown/blue areas representing cool spots/bright plages, the outer ticks mark the phases of observation. *Source*: Yu *et al.* (2017).

and brightness maps reconstructed from them. The brightness maps reconstructed for V830 Tau and the time-series of LSD profiles used for the fit are found in Donati *et al.* (2016) and Donati *et al.* (2017).

3. Looking for a planetary signature

After using ZDI to derive the surface brightness of both stars, revealing the presence of cool spots and warm plages, we applied three different methods to search for a planetary signature in the observed spectra. The first method studies the radial velocities filtered out from the activity jitter predicted by ZDI. The second method looks for the planet parameters that enable ZDI to fit the LSD profiles best, after having corrected them from the tested planet-induced reflex motion. The third method uses Gaussian-Process Regression (GPR) to fit the activity jitter in the raw RVs, and like the second method, searches for the orbital parameters which enable GPR to fit the raw RVs corrected from the reflex motion best.

ZDI #1. The first technique consists of using the previously reconstructed maps to predict the pollution to the RV curve caused by activity (called activity jitter in the following) and subtract it from the raw RVs. From the observed Stokes *I* LSD profiles, we compute the raw RVs RV_{raw}, as the first-order moment of the continuum-subtracted corresponding profiles. Likewise, the synthesised Stokes *I* LSD profiles derived from the brightness maps yield the synthesised activity jitter of the star (RV signal caused by the brightness distribution and stellar rotation). By subtracting the activity jitter from the raw RVs, we obtain filtered RVs RV_{filt} (see Fig. 2). Looking for a planet signature, we

https://doi.org/10.1017/S1743921317004264 Published online by Cambridge University Press

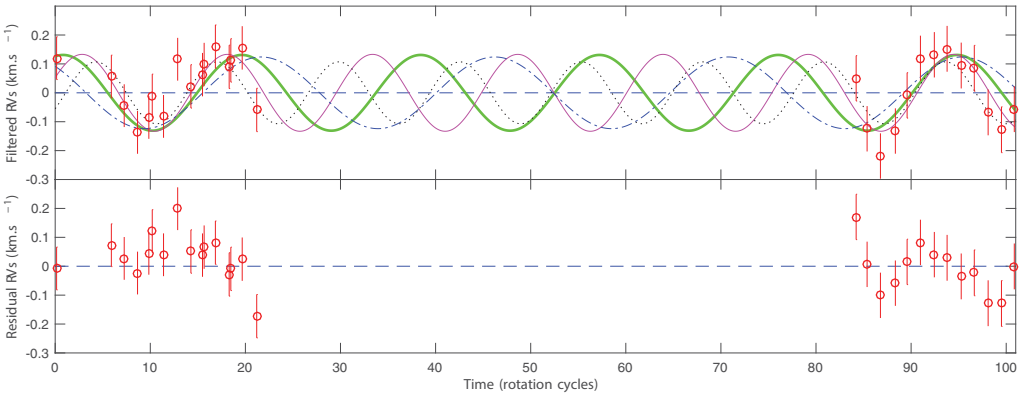

Figure 2. Top: filtered RVs of TAP 26 and four sine curves representing the best fits. The thick green curve represents the case $P_{\rm orb}/P_{\rm rot}$=18.80, the thin magenta one $P_{\rm orb}/P_{\rm rot}$=15.27, the dash-and-dotted blue one $P_{\rm orb}/P_{\rm rot}$=24.56 and the dotted black one $P_{\rm orb}/P_{\rm rot}$=12.76. Bottom: residual RVs resulting from the subtraction of the best fit (green curve) from the filtered RVs. The residual RVs feature a rms value of 51 m.s^{-1}.

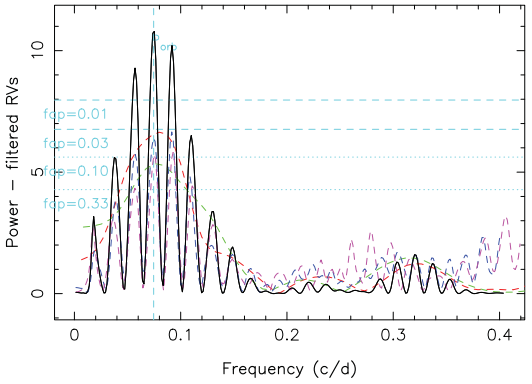

Figure 3. Periodogram of the TAP 26 filtered RV curve over the whole dataset (black line). The red line represents the 2015 Nov dataset, the green line the 2016 Jan dataset, the blue line the odd data points and the magenta line the even data points. False-alarm probability (FAP) levels of 0.33, 0.10, 0.03 and 0.01 are displayed as horizontal dashed cyan lines. The frequency that has the smallest FAP (0.06% at 0.075 cycles per day, corresponding to $P_{\rm orb}$=13.41 d) is marked by a cyan dashed line. Bottom: Zoom in the periodogram of filtered RVs.

want to fit a sine curve (of semi-amplitude K, period $P_{\rm orb}$, phase of inferior conjunction ϕ, and offset RV$_0$) to the RV$_{\rm filt}$, which corresponds to a circular orbit. The fitted curves are shown in Fig. 2 for TAP 26, and are found in Donati *et al.* (2016) and Donati *et al.* (2017) for V830 Tau. Plotting a Lomb-Scargle periodogram for the RV$_{\rm filt}$ further demonstrates the presence of a periodic signal (Fig. 3 for TAP 26, see Donati *et al.* 2016, Donati *et al.* 2017 for V830 Tau). By fitting the filtered RVs with a Keplerian orbit rather than a circular orbit, we obtain an eccentricity of 0.21±0.15 for V830 Tau and 0.16±0.15 for TAP 26, indicating that there is no evidence for an eccentric orbit following the precepts of Lucy & Sweeney (1971). We can thus conclude that the orbits of V830 Tau b and TAP 26 b are likely close to circular, or no more than moderately eccentric.

ZDI #2. In the previous method, we were trying to model the activity jitter by fitting data that were potentially the sum of both activity jitter and planet signature, leading to a risk of modelling part of the planet signature by brightness features on the reconstructed maps. To counter this, a next method is to add the presence of a planet into the physical

https://doi.org/10.1017/S1743921317004264 Published online by Cambridge University Press

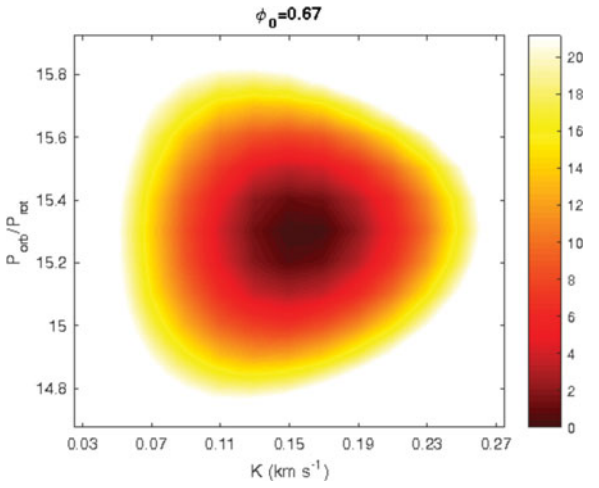

Figure 4. $\Delta\chi^2$ map as a function of K and $P_{\rm orb}/P_{\rm rot}$, derived with ZDI from corrected Stokes I LSD profiles at constant information content. Here the phase is fixed at 0.67, i.e., the value of ϕ at which the 3D paraboloid is minimum. The outer colour delimits the 99.99% confidence level area (corresponding to a χ^2 increase of 21.10 for 2581 data points in our Stokes I LSD profiles). The minimum value of $\chi^2_{\rm r}$ is 0.96824.

model and try to fit simultaneously the surface brightness and the planetary parameters to the LSD profiles. Technically, we try different values for the planetary parameters (amplitude K, period $P_{\rm orb}$ and phase ϕ of the RV signature, under the assumption of a circular orbit), and for each set of values, we subtract the planet-induced reflex motion from the spectra before applying ZDI to them. We look for the planet parameters that result in the best ZDI fit of the remaining activity jitter (see Petit *et al.* 2015, Yu *et al.* 2017). For both stars, we find consistent values of the planet parameters between methods #1 and #2 (Donati *et al.* 2017, Yu *et al.* 2017). A slice of the $\Delta\chi^2$ 3D-map, as a function of K, $P_{\rm orb}$ and ϕ, for TAP 26, is given on Fig. 4.

GPR. The third method we used works directly with the raw RVs and aims at modelling the activity jitter and its temporal evolution with GPR, assuming it obeys an a priori covariance function (Haywood *et al.* 2014, Rajpaul *et al.* 2015). Similarly to the previous method, we fit both the orbit model and the jitter model simultaneously. For a planet with given parameters, we first remove the planet-induced reflex motion from the RVs, then we fit the corrected RVs with a Gaussian process (GP) of pseudo-periodic covariance function:

$$c(t,t') = \theta_1^2 . \exp\left[-\frac{(t-t')^2}{\theta_3^2} - \frac{\sin^2\left(\frac{\pi(t-t')}{\theta_2}\right)}{\theta_4^2} \right] \tag{3.1}$$

where t and t' are two dates, θ_1 is the amplitude (in km.s^{-1}) of the GP, θ_2 the recurrence timescale (in units of $P_{\rm rot}$), θ_3 the decay timescale (i.e., the typical spot lifetime in the present case, in units of $P_{\rm rot}$) and θ_4 a smoothing parameter (within [0,1]) setting the amount of high frequency structures that we allow the fit to include. From a given set of orbital parameters (K, $P_{\rm orb}$, ϕ) and of covariance function parameters (θ_1 to θ_4, called hyperparameters), we can derive the GP that best fits the corrected RVs (noted y below) as well as the log likelihood $\log\mathcal{L}$ of the corresponding set of parameters from:

$$2\log\mathcal{L} = -n\log(2\pi) - \log|C+\Sigma| - y^T(C+\Sigma)^{-1}y \tag{3.2}$$

https://doi.org/10.1017/S1743921317004264 Published online by Cambridge University Press

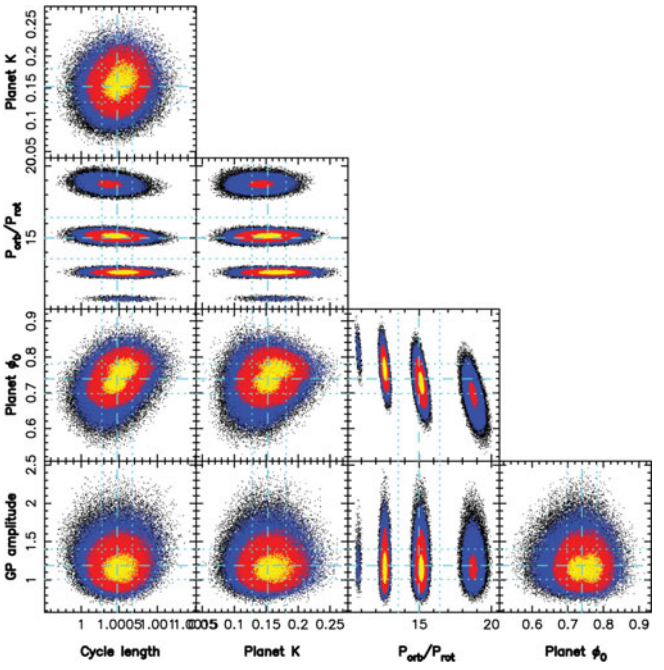

Figure 5. Phase plots of our 5-parameter MCMC run with yellow, red and blue points marking respectively the 1σ, 2σ and 3σ confidence regions. The optimal values found for each parameters are: θ_1=1.19±0.21 km.s^{-1}, θ_2=1.0005±0.0002 $P_{\rm rot}$, K=0.152±0.029 km.s^{-1}. Several optima are detected for $P_{\rm orb}$: 12.61±0.13 $P_{\rm rot}$, 15.12±0.20 $P_{\rm rot}$ and 18.74±0.34 $P_{\rm rot}$, ordered by decreasing likelihood. The corresponding phases ϕ are: 0.766±0.030, 0.728±0.033 and 0.694±0.042 respectively. *Source*: Yu *et al.* (2017).

where n is the number of data points, C is the covariance matrix of all the observing epochs and Σ is the diagonal variance matrix of the raw RVs. Coupled with a Markov Chain Monte Carlo (MCMC) simulation to explore the parameter domain, this method generates samples from the posterior probability distributions for the hyperparameters of the noise model and the orbital parameters. From these we can determine the maximum-likelihood values of these parameters and their uncertainty ranges. Fig. 5 shows the phase plot for TAP 26, where, after an initial run where all the parameters are free to vary, we fixed θ_4 and θ_3 to their respective best values (0.50±0.09 and 180±60 $P_{\rm rot}$=128±43 d) before carrying out the main MCMC run and looking for the best estimates of the 5 remaining parameters.

For both stars, GPR finds results that are consistent with those found using the ZDI methods.

4. Summary and discussion

All three methods demonstrate the clear presence of a planet signature in the data, although in the case of TAP 26 the gap between both data sets generates aliasing problems, causing multiple nearby peaks to stand out in the periodogram (of the dominant periods, the 10.8 d one emerges strongly for all three methods). Allowing ZDI to model temporal evolution of spot distributions and magnetic topologies should bring all methods on an equal footing; this upgrade is planned for a forthcoming study.

https://doi.org/10.1017/S1743921317004264 Published online by Cambridge University Press

The hJs in nearly circular orbits that we have discovered in the young systems V830 Tau and TAP 26 are better explained by type II disc migration than by planet-planet scattering coupled to tidal circularization. When compared to V830 Tau, a 2 Myr wTTS of $\simeq$1.0M$_\odot$, TAP 26, at $\simeq$17 Myr and of similar mass, appears as an evolved version, rotating 4x faster than its younger sister, likely as a direct consequence of its 4x smaller moment of inertia (according to the evolutionary models of Siess *et al.* 2000).

Regarding the hJs we detected around TAP 26 and V830 Tau and despite their differences (in mass in particular), it would be tempting to claim that, like its host star, TAP 26 b is an evolved version of V830 Tau b. This would actually imply that TAP 26 b migrated outwards under tidal forces from a distance of $\simeq$0.057 au (where V830 Tau b is located) to its current orbital distance of 0.094 au, as a result of the spin period of TAP 26 being $\simeq$15x shorter than the orbital period of TAP 26 b. This option seems however unlikely given the latest predictions of tidal interactions between a young T Tauri star and its close-in hot Jupiter (Bolmont & Mathis 2016), indicating that tidal forces can only have a significant impact on a hJ within 0.06 au of a solar-mass host star (for a typical TTS with a radius of $\simeq$2 R$_\odot$). The most likely explanation we see is thus that TAP 26 b:

- ended up its type-II migration in the accretion disc at the current orbital distance, when TAP 26 was still young, fully convective and hosting a large-scale dipole field of a few kG similar to that of AA Tau (Donati *et al.* 2010), i.e., strong enough to disrupt the disc up to a distance of 0.09 au,
- was left over once the disc has dissipated at an age significantly smaller than 2 Myr, i.e., before the large-scale field had time to evolve into a weaker and more complex topology, and the inner accretion disc to creep in as a result (e.g., Blinova *et al.* 2016).

Admittedly, this scenario requires favorable conditions to operate; in particular, it needs the accretion disc to vanish in less than 2 Myr, which happens to occur in no more than 10% of single T Tauri stars in Taurus (Kraus *et al.* 2012). In fact, since both TAP 26 and V830 Tau have the same angular momentum content, it is quite likely that TAP 26 indeed dissipated its disc very early. Quantitatively speaking, assuming (i) that the hJ we detected tracks the location of the inner disc when the disc dissipated, (ii) that the spin period at this time was locked on the Keplerian period of the inner disc (equal to the orbital period of the detected hJ) and (iii) that stellar angular momentum was conserved since then, we derive that the disc must have dissipated when TAP 26 was about three times larger in radius, at an age of less than 1 Myr (according to Siess *et al.* 2000). Generating a magnetospheric cavity of the adequate size would have required TAP 26 to host at this time a large scale dipole field of 0.3-1.0 kG for mass accretion rates in the range 10^{-9} to 10^{-8} M$_\odot$ /yr, compatible with the large-scale fields found in cTTSs of similar masses (e.g., GQ Lup, Donati *et al.* 2012).

Along with other recent reports of close-in giant planets (or planet candidates) detected (or claimed) around young stars (van Eyken *et al.* 2012, Mann *et al.* 2016, Johns-Krull *et al.* 2016, David *et al.* 2016), our results may suggest a surprisingly high frequency of hJs around young solar-type stars, with respect to that around more evolved stars ($\simeq$1%, Wright *et al.* 2012). However, this may actually reflect no more than a selection bias in the observation samples (as for their mature equivalents in the early times of velocimetric planet detections). Planets are obviously much easier to detect around non-accreting TTSs as a result of their lower level of intrinsic variability; observation samples (like that of MaTYSSE) are thus naturally driven towards young TTSs whose accretion discs vanished early, i.e., at a time when their large-scale fields were still strong and their magnetospheric gaps large, and thus for which hJs had more chances to survive

https://doi.org/10.1017/S1743921317004264 Published online by Cambridge University Press

type-II migration. A more definite conclusion must wait for a complete analysis of the full MaTYSSE sample.

More observations are currently being planned to better determine the characteristics of the newborn hJs we detected. Furthermore, analyzing thoroughly the full MaTYSSE data set to pin down the frequency of newborn hJs within the sample observed so far will bring a clearer view on how the formation and migration of young giant planets is occurring. Ultimately, only a full-scale planet survey of young TTSs such as that to be carried out with SPIRou, the new generation spectropolarimeter currently being built for CFHT and scheduled for first light in 2018, will be able to bring a consistent picture of how young close-in planets form and migrate, how their population relates to that of mature hJs, and more generally how young hJs impact the formation and early architecture of planetary systems like our Solar System.

References

Baruteau, C. *et al.* 2014, *Protostars and Planets VI*, pp. 667–689
Batygin, K., Bodenheimer, P. H., & Laughlin, G. P. 2016, *ApJ*, 829, 114
Blinova, A. A., Romanova, M. M., & Lovelace, R. V. E. 2016, *MNRAS*, 459, 2354
Bolmont, E. & Mathis, S. 2016, *Celestial Mechanics and Dynamical Astronomy*, 126, 275
Brown, S. F., Donati, J.-F., Rees, D. E., & Semel, M. 1991, *A&A*, 250, 463
David, T. J. *et al.* 2016, *Nature*, 534, 658
Donati, J.-F., Semel, M., Carter, B. D., Rees, D. E., & Collier Cameron, A. 1997, *MNRAS*, 291, 658
Donati, J.-F. & Brown, S. F. 1997, *A&A*, 326, 1135
Donati, J.-F. *et al.* 2006, *MNRAS*, 370, 629
Donati, J.-F. *et al.* 2008, *MNRAS*, 385, 1179
Donati, J. *et al.* 2010, *MNRAS*, 409, 1347
Donati, J.-F. *et al.* 2012, *MNRAS*, 425, 2948
Donati J.-F. *et al.* 2014, *MNRAS*, 444, 3220
Donati, J.-F. *et al.* 2015, *MNRAS*, 453, 3706
Donati, J.-F. *et al.* 2016, *Nature*, 534, 662
Donati, J.-F. *et al.* 2017, *MNRAS*, 465, 3343
van Eyken, J. C. *et al.* 2012, *ApJ*, 755, 42
Haywood, R. D. *et al.* 2014, *MNRAS*, 443, 2517
Huélamo, N. *et al.* 2008, *A&A*, 489, L9
Johns-Krull, C. M. *et al.* 2016, *ApJ*, 826, 206
Kraus, A. L., Ireland, M. J., Hillenbrand, L. A., & Martinache, F. 2012, *ApJ*, 745, 19
Lagrange, A.-M. *et al.* 2010, *Science*, 329, 57
Lucy, L. B. & Sweeney, M. A. 1971, *AJ*, 76, 544
Mann, A. W. *et al.* 2016, *AJ*, 152, 61
Moutou, C. *et al.* 2007, *A&A*, 473, 651
Rajpaul, V., Aigrain, S., Osborne, M. A., Reece, S., & Roberts, S. 2015, *MNRAS*, 452, 2269
Sallum, S. *et al.* 2015, *Nature*, 527, 342
Semel, M. 1989, *A&A*, 225, 456
Setiawan, J., Henning, T., Launhardt, R., Müller, A., Weise, P., & Kürster, M. 2008, *Nature*, 451, 38
Siess, L., Dufour, E., & Forestini, M. 2000, *A&A*, 358, 593
Vogt, S. S., Penrod, G. D., & Hatzes, A. P. 1987, *ApJ*, 321, 496
Wright, J. T., Marcy, G. W., Howard, A. W., Johnson, J. A., Morton, T. D., & Fischer, D. A. 2012, *ApJ*, 753, 160
Yu, L. *et al.* 2017, *MNRAS*, 467, 1342

https://doi.org/10.1017/S1743921317004264 Published online by Cambridge University Press